BNL-96170-2011-JA

Mechanical Performance of the LARP Nb_3Sn Quadrupole Magnet LQS01

P. Ferracin, G. Ambrosio, M. Anerella, B. Bingham, R. Bossert, S. Caspi, D. W. Cheng, G. Chlachidze, H. Felice, A. R. Hafalia, W. Mumper, F. Nobrega, S. Prestemon, G. L. Sabbi, J. Schmalzle, C. Sylvester, M. Tartaglia, P. Wanderer, and A. V. Zlobin

***Abstract*—As part of the effort towards the development of Nb_3Sn magnets for future LHC luminosity upgrades, the LHC Accelerator Research Program (LARP) has fabricated and tested the quadrupole magnet LQS01. The magnet implements 3.4 m long Nb_3Sn coils contained in a support structure characterized by an external aluminum shell segmented in four sections. The room temperature pre-load of the structure is obtained by shimming load keys through bladders, pressurized during the loading operations and removed before cool-down. Temperature compensated strain gauges, mounted on structure components and coil poles, monitor the magnet's mechanical behavior during assembly, cool-down and, excitation. During the first test, LQS01 reached the target gradient of 200 T/m; the gauge data indicated that the aluminum shell was pre-tensioned to the target value estimated by numerical models, but a lack of pre-load was measured in the coil inner layer during ramping. As a result, the test was interrupted and the magnet disassembled, and inspected. A second test (LQS01b) was then carried out following a re-loading of the magnet. The paper reports on the strain gauge results of the first test and the analysis performed to identify corrective actions to improve the coil pre-stress distribution. The mechanical performance of the magnet during the second cool-down and test is then presented and discussed.**

***Index Terms*—LARP, Nb_3Sn, quadrupole magnet.**

I. Introduction

THE QUADRUPOLE magnet LQS01 has been developed by the US LHC Acceleration Research Program (LARP, [1]–[3]) with the goal of demonstrating that quadrupoles based on Nb_3Sn technology and in lengths compatible with accelerator-type magnets can be adopted in future luminosity upgrades of the LHC. The LQS01 design, a 3.7 m long scale-up of the 1 m long TQS magnet design [4], features four double-layer cos-theta coils, fabricated at FNAL and BNL [5], contained by a support structure designed and assembled at LBNL [6].

Manuscript received August 03, 2010; accepted December 01, 2010. Date of publication January 06, 2011; date of current version May 27, 2011. This work was supported by the Director, Office of Energy Research, Office of High Energy and Nuclear Physics, High Energy Physics Division, U.S. Department of Energy, under Contract DE-AC02-05CH11231.

P. Ferracin, B. Bingham, S. Caspi, D. W. Cheng, H. Felice, A. R. Hafalia, S. Prestemon, and G. L. Sabbi are with the Lawrence Berkeley National Laboratory, Berkeley, CA 94720 USA (e-mail: pferracin@lbl.gov).

G. Ambrosio, R. Bossert, G. Chlachidze, W. Mumper, F. Nobrega, C. Sylvester, M. Tartaglia, and A.V. Zlobin are with the Fermilab National Accelerator Laboratory, Batavia, IL 60510 USA.

M. Anerella, J. Schmalzle, and P. Wanderer are with the Brookhaven National Laboratory, Upton, NY 11973-5000 USA.

Color versions of one or more of the figures in this paper are available online at http://ieeexplore.ieee.org.

Digital Object Identifier 10.1109/TASC.2010.2097571

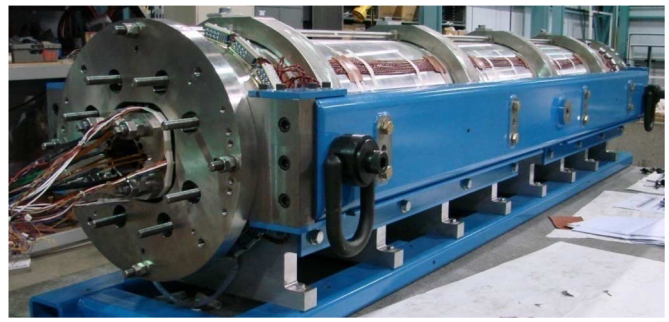

Fig. 1. LQS01a after assembly and loading.

The LQS01 target performance, set in the early stages of the LARP Program, is to reach in a 90 mm aperture a gradient of 200 T/m, corresponding to 80% of the 4.5 K maximum ("short-sample") gradient G_{ss}, and to reproduce the quench performance of the TQS program [7]. In 2009, LQS01 was assembled and loaded at LBNL (Fig. 1), following the procedure described in [5], [8]. The magnet was then shipped to FNAL, cooled-down, and tested as LQS01a. During assembly and test, the strain gauges mounted on the coil titanium-alloy poles indicated that the coil compression was lower than expected and inconsistent with the stress of the support structure. After the test, LQS01a was therefore shipped back to LBNL for a full disassembly and inspection. Modifications were implemented to the structure in order to improve coil stresses, and the performance was verified in a second test (LQS01b) carried out at FNAL. We provide here an overview of the LQS01 mechanical performance, starting with gauge measurements taken during LQS01a test and proceeding with a description of finite element model results and of the corrective strategies applied to the support structure. We conclude with the results of the LQS01b test and a comparison of quench performances.

II. Magnet Design and Parameters

The LQS01 magnet cross-section, shown in Fig. 2 (left), is characterized by four iron pads surrounding the coils and four iron yokes. The yoke quadrants are separated by open gaps and contained within an outer aluminum shell. The shell, axially segmented in 4 sections 0.8 m long, is pre-loaded with water pressurized bladders inserted between pads and yokes. In the end region, the coils are supported in the longitudinal direction by stainless steel end plates connected by four stainless steel rods, pre-tensioned with a hydraulic piston (Fig. 2, right). The expected limit conditions at 4.5 K and 1.9 K, based on strand measurements, are given in Table I.

U.S. Government work not protected by U.S. copyright.

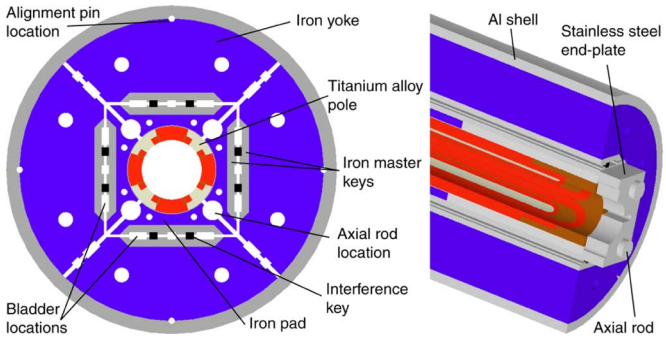

Fig. 2. LQS01 magnet cross-section (left) and end design (right).

TABLE I
CABLE AND MAGNET PARAMETERS

Parameter	Unit	
Short sample current I_{ss} at 4.5 / 1.9 K	kA	13.75 / 15.31
Gradient at I_{ss} at 4.5 / 1.9 K	T/m	240 / 265
Coil peak field (layer 1) at I_{ss} at 4.5 / 1.9 K	T	12.28 / 13.56
Stored energy at I_{ss} at 4.5 / 1.9 K	kJ/m	473 / 570
Inductance	mH/m	4.9

Values computed based on extracted strand measurements (J_c = 2720 A/mm^2 at 4.2 K and 12 T), assuming a self-field correction of 0.483 T/kA.

III. MECHANICAL PERFORMANCE

The mechanical performance of LQS01 was monitored from assembly to excitation with strain gauges mounted on aluminum shell, axial rods, and coil titanium-alloy poles. The shell was instrumented with half-bridge strain gauges placed on each of the four segments ("S1" to "S4" from the lead end), and distributed on four mid-planes ("T" top, "R" right, "B" bottom, and "L" left). Each gauge was thermally compensated by a second gauge mounted on a stress-free aluminum element and both the azimuthal ("T") and axial strain ("Z") was recorded. A similar configuration was adopted for the coils' ("C") titanium-alloy poles, instrumented on the inner layer with azimuthal ("T") and axial ("Z") gauges mounted along four axial locations ("1" to "4" from the lead end). In addition, each axial rod was equipped with two half-bridge gauges mounted in opposite azimuthal locations to compensate for bending effects. In total, 56 gauges were mounted on LQS01 and their measurements were compared with numerical expectations from a 3D finite element model of the entire magnet geometry.

Both the computed and measured average (± 1 standard deviation) values of strain and stress for LQS01a and LQS01b are shown in Tables II and III, and they will be discussed in the following sub-sections.

A. LQS01a

The evolution of the stress in shell, rods, and poles from the end of the LQS01a room-temperature pre-loading operations to the conditions after cool-down are shown in Figs. 3–5. The target (computed) values, depicted in the figure and given in Table II, were chosen according to finite element model results and represent the estimated pre-load levels required to avoid separation between coil and pole up to a gradient of 230–240 T/m. In LQS01a, the aluminum shell was pre-tensioned during the bladder operation to $+35 \pm 10$ MPa and it reached at 4.5 K an azimuthal stress of $+150 \pm 5$ MPa, consistent with calculations (Fig. 3). The large variations of stress measured in the segment located at the bottom of the cryostat occurred during cool-down when liquid helium was poured into the cryostat. The axial rods, tensioned to the target value with a hydraulic piston, experienced a stress variation during cool-down from $+60 \pm 5$ MPa to $+200 \pm 10$ MPa, also in agreement with model results (Fig. 4). Unlike shell and rod data, a discrepancy was observed between measured and expected azimuthal pole pre-load at end of bladder operation, as if the compressive force provided by the shell was not reaching the coil inner layer (Fig. 5).

The same inconsistency was then recorded at the end of the cool-down, with a measured pole compression of -25 ± 20 MPa, compared to the -120 MPa estimated by the model. Confirming this low coil pre-load level, most of the pole gauges showed during current ramps a "stress knee" (Fig. 6), followed by a "stress plateau". This stress profile is usually interpreted as a sign of coil-pole separation. A further observation could be made based on the pole gauge data during ramps: when the coil separates from the pole, the stress in the pole has

TABLE II
LQS01A COMPUTED AND MEASURED ($\pm 1\sigma$) STRAIN AND STRESS IN SHELL, POLES, AND AXIAL RODS

293 K	ε_y (μstrain)	ε_z (μstrain)	σ_y (MPa)	σ_z (MPa)
Shell comp.	+450	-70	+35	+5
Shell meas.	+460 ±110	-100 ±110	+35 ±10	+5 ±10
Pole comp.	-345	+10	-50	-15
Pole meas.	-20 ±70	+140 ±160	+5 ±10	+20 ±20
Rod comp.	n/a	+330	n/a	+60
Rod meas.	n/a	+310 ±20	n/a	+60 ±5
4.5 K	ε_y (μstrain)	ε_z (μstrain)	σ_y (MPa)	σ_z (MPa)
Shell comp.	+1750	-60	+155	+50
Shell meas.	+1630 ±120	+30 ±200	+150 ±5	+50 ±15
Pole comp.	-780	-240	-120	-70
Pole meas.	-180 ±100	0 ±260	-25 ±20	-5 ±35
Rod comp.	n/a	+1015	n/a	+215
Rod meas.	n/a	+940 ±50	n/a	+200 ±10

TABLE III
LQS01B COMPUTED AND MEASURED ($\pm 1\sigma$) STRAIN AND STRESS IN SHELL, POLES, AND AXIAL RODS

293 K	ε_y (μstrain)	ε_z (μstrain)	σ_y (MPa)	σ_z (MPa)
Shell comp.	+750	-120	+55	+10
Shell meas.	+860 ±100	-190 ±100	+65 ±5	+8 ±7
Pole comp.	-580	+20	-80	-20
Pole meas.	-840 ±160	+120 ±100	-115 ±25	-15 ±15
Rod comp.	n/a	+340	n/a	+65
Rod meas.	n/a	+470 ±15	n/a	+90 ±3
4.5 K	ε_y (μstrain)	ε_z (μstrain)	σ_y (MPa)	σ_z (MPa)
Shell comp.	+2080	-70	+185	+60
Shell meas.	+2150 ±125	+180 ±300	+200 ±10	+85 ±20
Pole comp.	-1030	-200	-160	-75
Pole meas.	-900 ±180	-60 ±175	-130 ±30	-45 ±30
Rod comp.	n/a	+1030	n/a	+220
Rod meas.	n/a	+1140 ±40	n/a	+240 ±10

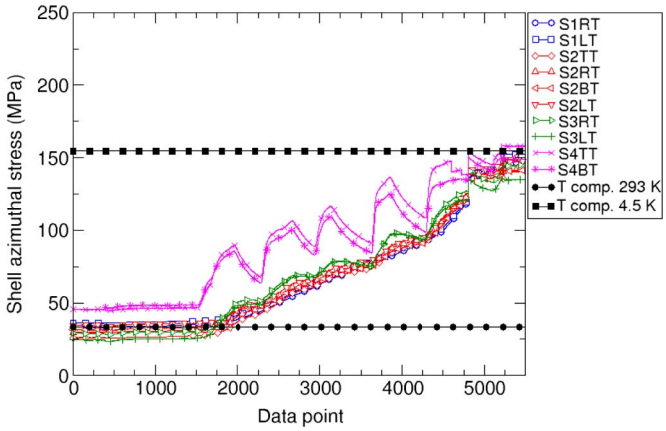

Fig. 3. Measured and computed azimuthal (T) stress on the shell during LQS01a cool-down vs. data point.

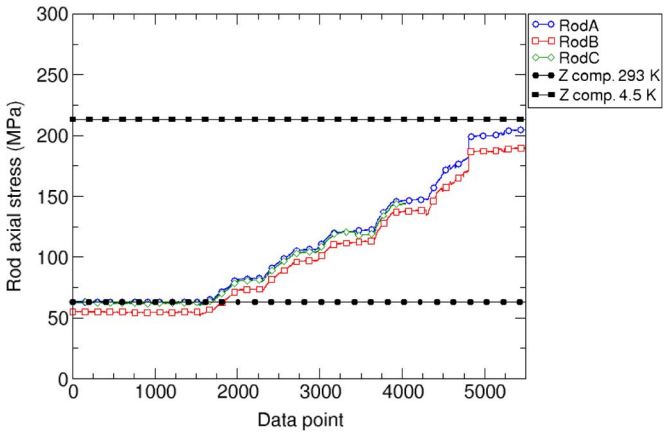

Fig. 4. Measured and computed axial (Z) stress on the rods during LQS01a cool-down vs. data point.

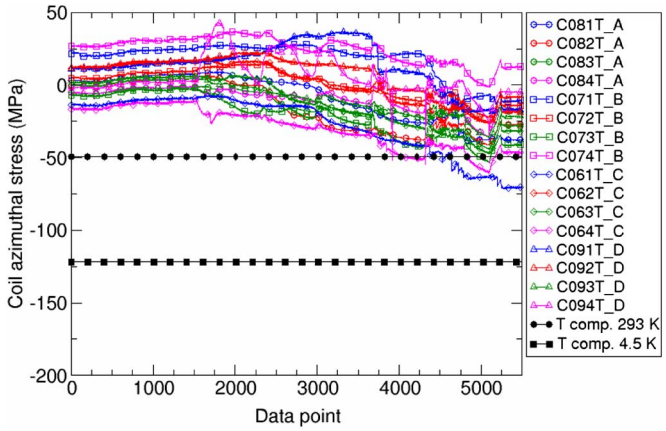

Fig. 5. Measured and computed azimuthal (T) stress on the coil poles during LQS01a cool-down vs. data point.

to be equal to zero. As a result, the stress plateau in Fig. 6 can be used to re-calibrate the offsets of the gauges. According to the new offsets, the average stress in the poles before excitation ranged from -50 to -100 MPa. This values, different from the -25 MPa recorded after cool-down, constituted a second inconsistency of the gauge data at cryogenic temperature.

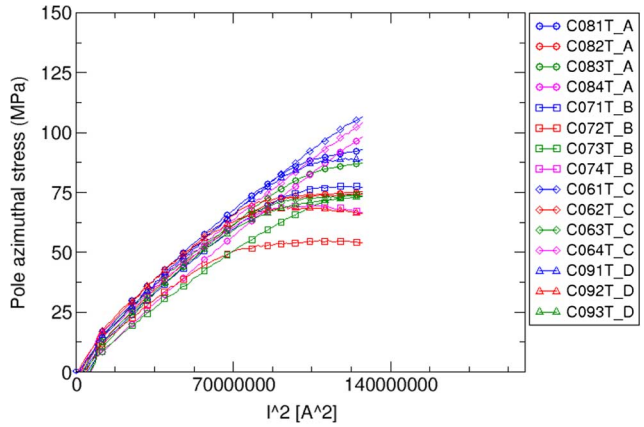

Fig. 6. Measured variation of azimuthal (T) stress on the coil poles during excitation from 0 to 11.4 kA vs. $I^2[A^2]$ in LQS01a test.

B. Analysis and Structure Modifications

After the LQS01a test, the magnet was unloaded and disassembled at LBNL, and a full investigation was launched with the goal of understanding the inconsistencies between measured and expected coil strain, and defining a set of structure modifications to improve stress distribution. A first area of investigation regarded coil dimensional measurements. In [8] it was pointed out that a possible cause for the low pre-compression on the coil inner layer could be related to discrepancies in coil dimensions with respect to the design geometry. Indeed, dimensional measurements performed at BNL and FNAL confirm that the LQ coils are oversized in the azimuthal direction due to a shift of the mid-plane of about $+0.100 \pm 0.050$ mm [9]. To evaluate the impact of the mid-plane shift, we computed the coil stress profile with an additional shim on the mid-plane. The results, compared with reference conditions, are shown in Fig. 7, where the deformed shapes before and after pre-loading are plotted, and the mid-plane shim is simulated as a displacement between coils.

In the nominal case (left plots), the pre-loading operation starts with the coil outer radius perfectly matching the pad inner radius (top left plot). When bladders are pressurized, the pads are pushed against the coil, transferring the compressive force both to the conductor blocks and to the poles. In the case of the oversized coil (right plots), the mid-plane shim determines a mismatch between coil outer surface and pad inner surface, and contact occurs only in the pole area (top right plot).

As a result, the final coil shape features a larger radial displacement in the pole region than in the mid-plane region (bottom right plot).

Fig. 7 demonstrates that the final stress distribution within the coil layers can vary depending on the contact with the pads, even if the force coming from the structure is the same. The same conclusion can be drawn from the model results shown in Fig. 8, where the strain in the pole (gauge location) is plotted as a function of the shell tension. The solid line represents the computed nominal conditions, featuring, as expected, a linear increase of pole compression with increasing shell tension. The dashed line shows the strain conditions with an oversized coil: in the initial part of the loading, a significant fraction of the force is used to create full contact between coil and pad, and

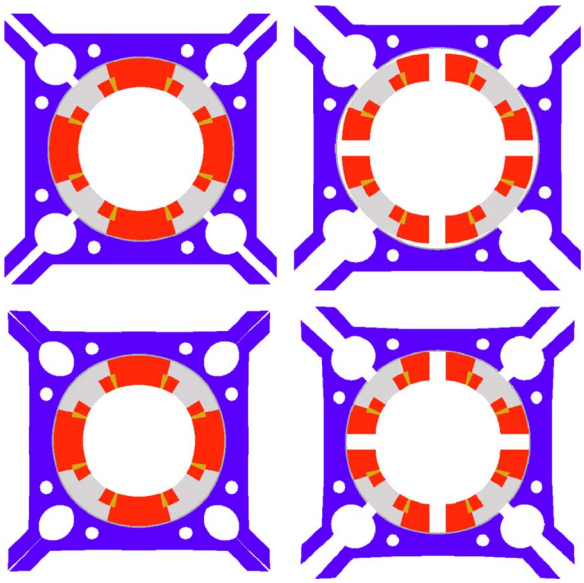

Fig. 7. Computed deformed shape of the LQS01 coil-pad sub-assembly before (top) and after (bottom) pre-loading, in nominal conditions (left) and with an oversized coil (right). Displacements are enhanced by a factor 50.

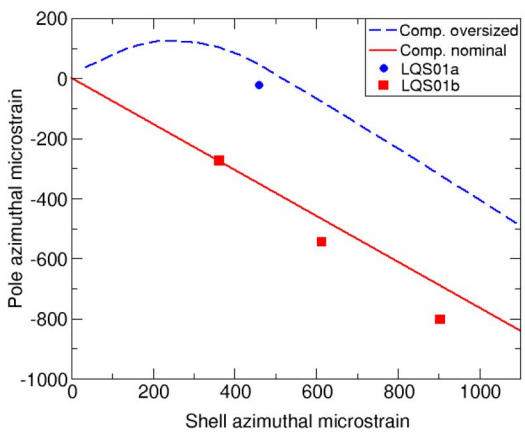

Fig. 8. Pole azimuthal strain vs. shell azimuthal strain during room-temperature pre-loading: computed values in nominal conditions (solid line) and with an oversized coil (dashed line), and measured values in LQS01a (round marker) and LQS01b (square markers).

only a marginal variation of pole compression in the inner layer is produced. The pole strain starts decreasing with the nominal rate only once full contact is established between coil and pad. With a mid-plane shim of 0.120 mm included in the model, the computations are consistent with LQS01a measurements taken at the end of the bladder operation (round marker).

Based on the results of the investigation, it was decided to apply two modifications to LQS01b structure and loading. The thickness of the G10 shim providing electrical insulation between coil and pad was reduced from 0.765 mm to 0.380 mm, with the purpose of effectively increasing the pad inner radius and improving the coil-pole contact uniformity. Pressure sensitive film tests, performed before final assembly, confirmed the improvement in coil-pad contact uniformity. In addition, the final room-temperature shell pre-load was increased, to further mitigate the risk of low coil pre-stress. As a result, the measurements of the strain in poles and shell during LQS01b bladder

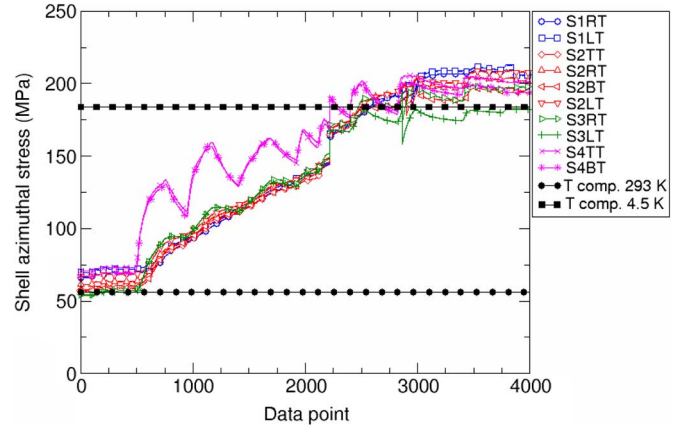

Fig. 9. Measured and computed azimuthal (T) stress on the shell during LQS01b cool-down vs. data point.

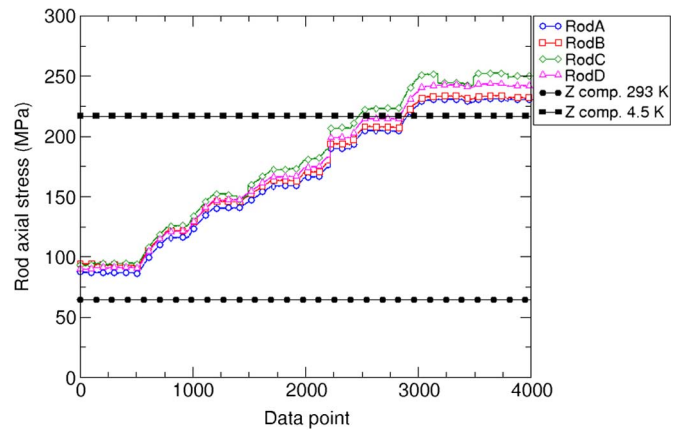

Fig. 10. Measured and computed axial (Z) stress on the rods during LQS01b cool-down vs. data point.

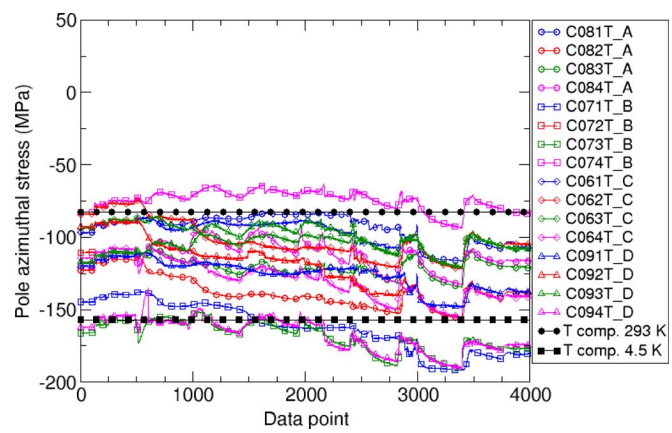

Fig. 11. Measured and computed azimuthal (T) stress on the coil poles during LQS01b cool-down vs. data point.

operation (Fig. 8, square markers) were in agreement with expected nominal values.

C. LQS01b

The stresses in shell, rods, and poles during LQS01b cool-down are shown in Figs. 9–11. At 4.5 K, the shell reached a tension of $+200 \pm 10$ MPa, about 50 MPa more than in LQS01a, while the rod was tensioned to $+240 \pm 10$ MPa ($+200 \pm 10$ MPa

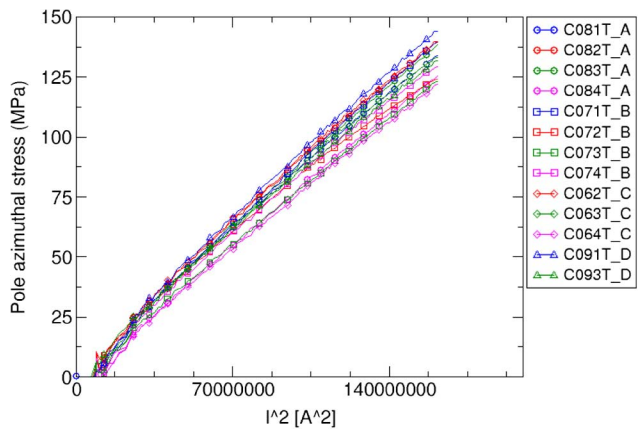

Fig. 12. Measured variation of azimuthal (T) stress on the coil poles during excitation from 0 to 12.8 kA vs. $I^2[A^2]$ in LQS01b test.

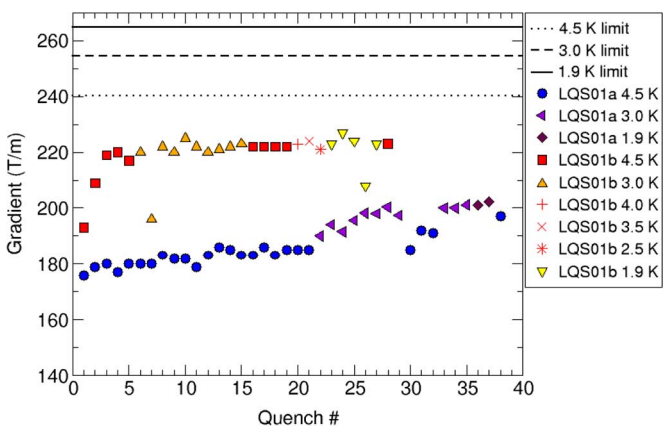

Fig. 13. Gradient (T/m) vs. training quenches with a ramp rate $\leq$20 A/s.

in LQS01a). As a result of the structure modifications and the choice of a higher stress target, the pole pre-load after cool-down went from -25 ± 20 MPa in LQS01a to -130 ± 30 MPa in LQS01b, and no separation was observed between coil and pole during excitation (Fig. 12).

It is important to point out that, in term of variation of coil pre-load during cool-down, LQS01b exhibited the same discrepancy with numerical expectation as LQS01a. A clear explanation for this behavior has not been found yet, and the data cannot be reproduced by finite element models. A possible cause, still under investigation, may reside on an error in the temperature compensation.

IV. Quench Performance

The training histories of the two LQS01 tests are shown in Fig. 13 and Fig. 14, where the gradient and fraction of short sample limits is plotted for all the low ($\leq$20 A/s) ramp-rate quenches. Details of the tests can be found in [10], [11].

LQS01a had a first quench at 4.5 K with a gradient of 176 T/m, corresponding to 71% of the short sample gradient G_{ss}. After 37 quenches and two cool-downs to 3 K, LQS01a reached the maximum gradient of 202 T/m at 1.9 K. In the last quench (#38), carried out a temperature of 4.5 K, a gradient of 197 T/m (81% of G_{ss}) was achieved. At the time of the submission of this paper the first thermal cycle of the LQS01b test was completed. After four quenches, LQS01b

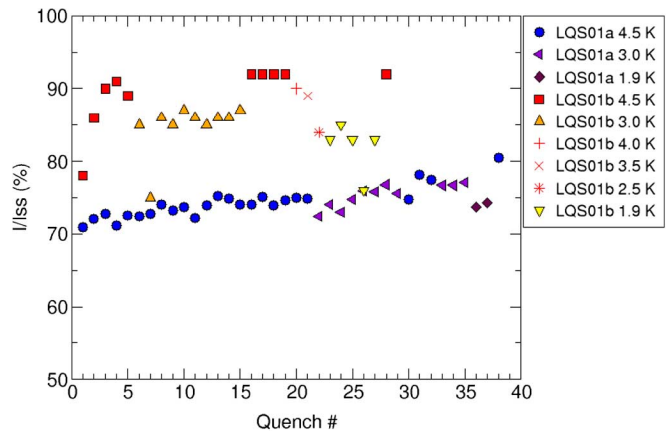

Fig. 14. Short-sample % vs. training quenches with a ramp rate $\leq$20 A/s.

reached a plateau at a gradient level of 220 T/m. The maximum gradient of 227 T/m and the maximum fraction of short-sample of 92% were achieved respectively at 1.9 K and 4.5 K.

V. Conclusions

The mechanical performance of the LARP Nb_3Sn quadrupole magnet LQS01, a 3.7 m long scale-up of the 1 m long TQS magnet, was presented. During the first test (LQS01a), the magnet reached the target gradient of 200 T/m but a low pre-load was measured in the coil inner layer. An investigation focuses on coil dimensional measurements and numerical models identified a mismatch of the contact surfaces between coil and support structure. Following an optimization of the structure and an increase in pre-stress at 293 K, the magnet was retested as LQS01b and an improved performance was recorded: a gradient of 227 T/m and a fraction short-sample of 92% were reached, and the performance of the best short model (TQS02c) reproduced.

References

[1] S. A. Gourlay *et al.*, "Magnet R&D for the IS LHC accelerator research program," *IEEE Trans. Appl. Supercond.*, vol. 16, no. 2, pp. 324–327, June 2006.

[2] P. Wanderer, "Overview for LARP magnet R&D," *IEEE Trans. Appl. Supercond.*, vol. 19, no. 3, pp. 1208–1211, June 2009.

[3] P. Ferracin, "LARP Nb_3Sn quadrupole magnets for the LHC luminosity upgrade," in *AIP Conf. Proc.*, 2010, vol. 1218, pp. 1291–1300.

[4] S. Caspi *et al.*, "Fabrication and test of TQS01—A 90 mm Nb_3Sn quadrupole magnet for LARP," *IEEE Trans. Appl. Supercond.*, vol. 17, no. 2, pp. 1122–1125, June 2007.

[5] G. Ambrosio *et al.*, "Development and coil fabrication for the LARP 3.7-m long Nb_3Sn quadrupole," *IEEE Trans. Appl. Supercond.*, vol. 19, no. 3, pp. 1231–1234, June 2009.

[6] P. Ferracin *et al.*, "Fabrication and test of a 3.7 m long support structure for the LARP Nb_3Sn quadrupole magnet LQS01," *IEEE Trans. Appl. Supercond.*, vol. 19, no. 3, pp. 1106–1111, June 2009.

[7] S. Caspi *et al.*, "Test results of LARP Nb_3Sn quadrupole magnets using a shell-based support structure (TQS)," *IEEE Trans. Appl. Supercond.*, vol. 19, no. 3, pp. 1221–1225, June 2009.

[8] P. Ferracin *et al.*, "Assembly and loading of LQS01, a shell-based 3.7 m Long Nb_3Sn quadrupole magnet for LARP," *IEEE Trans. Appl. Supercond.*, vol. 20, no. 3, pp. 279–282, June 2010.

[9] G. Ambrosio, *Private Communications*. FNAL.

[10] G. Ambrosio *et al.*, "Final development and test preparation of the first 3.7 m long Nb_3Sn quadrupole by LARP," *IEEE Trans. Appl. Supercond.*, vol. 20, no. 3, pp. 283–287, June 2010.

[11] G. Ambrosio *et al.*, "Test results of the first 3.7 m long Nb_3Sn quadrupole by LARP and future plans," *IEEE Trans. Appl. Supercond.*, submitted for publication.